

WI4680 Applications in Partial Differential Equations

## Assignments

Philip Soliman (4945255)

June 23, 2024



**Supervisor:**

Dr. H.M. Schuttelaars

Delft University of Technology

Faculty of Electrical Engineering, Mathematics and

Computer Science

# Contents

Introduction . . . . .	3
Assignment 1 . . . . .	4
1.1 Boundary Conditions . . . . .	4
1.2 Discretisation . . . . .	5
1.3 Derivation: exact vs. numerical . . . . .	5
1.4 Finding equilibria: Newton and Broyden . . . . .	6
1.5 Embedding . . . . .	7
1.6 Bifurcation diagrams . . . . .	7
1.7 Conclusion . . . . .	9
Assignment 2 . . . . .	10
2.1 Stationary points . . . . .	10
2.2 Continuation of stationary points . . . . .	11
2.3 Continuation of limit cycle from Hopf-bifurcation . . . . .	13
2.4 Period doubling bifurcations . . . . .	14
2.5 Route to chaos . . . . .	16
2.6 Conclusion . . . . .	16
Assignment 3 . . . . .	17
3.1 Introduction . . . . .	17
3.2 Autonomous system . . . . .	17
3.3 Non-autonomous system . . . . .	19
3.4 R-tipping . . . . .	21
3.5 Conclusion . . . . .	23

## **Introduction**

This report contains my treatment of the assignments. It will be updated as I progress through the course.

All my code is available [here](#).

# Assignment 1

The goal of this assignment is to find the equilibria of a energy balance equation based on a very simplified model of the Earth. Additionally, we perform a one parameter analysis using continuation on a parameter that represents the greenhouse effect. This allows us to study the bifurcation diagram of the model.

Variable	Unit	Meaning	Value
$\theta$	-	latitude	$[-\frac{\pi}{2}, \frac{\pi}{2}]$
$t$	s	time	-
$x = \sin \theta$	-	latitude coordinate	$[-1, 1]$
$T$	K	temperature	-
$R_A$	$J s^{-1} m^{-2}$	effective solar radiation	-
$Q$	$J s^{-1} m^{-2}$	solar radiation	-
$Q_0$	$J s^{-1} m^{-2}$	solar radiation constant	341.3
$\alpha$	-	albedo of Earth	-
$\alpha_1$	-	albedo of ice	0.7
$\alpha_2$	-	albedo of water	0.289
$T^*$	K	temperature at which ice melts	273.15
$M$	$K^{-1}$	temperature gradient (?)	-
$\mu$	$J s^{-1} m^{-2}$	greenhouse gas & fine particle parameter	30
$R_E$	$J s^{-1} m^{-2}$	black body radiation	-
$h_0$	-	emmissivity of Earth	0.61
$\sigma_0$	$J s^{-1} m^{-2} K^{-4}$	Stefan-Boltzmann constant	$5.67 \cdot 10^{-8}$
$R_D$	$J s^{-1} m^{-2}$	heat dispersion	-
$D$	$J s^{-1} m^{-2}$	heat dispersion constant	0.3
$\delta$	$J s^{-1} m^{-2}$	heat dispersion at poles	0
$C_T$	$JK^{-1}$	heat capacity of Earth	$5 \cdot 10^8$

Table 1: Variables and their meanings

## 1.1 Boundary Conditions

$\delta$  cannot be positive (resp. negative) at  $x = \pm 1$  (poles), otherwise energy would be artificially entering (resp. leaving) the system. Simply said, the poles cannot be a source or sink of energy. This requires us to set  $\delta = 0$  at  $x = \pm 1$ . Furthermore

$$\left. \frac{dT}{dx} \right|_{x=\pm 1} = 0.$$

However, we run into a problem when we combine the boundary conditions and set  $\delta = 0$ . The equation for the heat dispersion vanishes at the boundary and we are left with two algebraic equations in terms of  $T(\pm 1)$

$$R_A(T, x) - R_E(T)|_{x=\pm 1} = 0.$$

Solving these equations for  $T(\pm 1)$  gives us the equilibrium temperature at the poles

$$T_{eq}(\pm 1) \approx 220.5K,$$

for the values specified in table 1.

Alternatively, we can resort to a more basic requirement. Namely, that there must exist an equilibrium temperature  $T_0$  at the poles,

$$\begin{aligned} F(T(x, t))|_{x=\pm 1} &= 0, \quad \forall t > 0, \\ \implies -2x \frac{dT}{dx} + R_A - R_E &\Big|_{x=\pm 1} = 0. \end{aligned}$$

Assuming we use the given expansion of  $T$  in terms of legendre polynomials, we can write the above as

$$\begin{aligned} \sum_{n=0}^{\infty} 2x \frac{\lambda_n}{D} a_n \frac{d\phi_n}{dt} - (R_A - R_E) &\Big|_{x=\pm 1} = 0, \\ \implies \begin{cases} \sum_{n=0}^{\infty} \frac{\lambda_n^2 a_n}{D} = R_A - R_E|_{x=1}, \\ \sum_{n=0}^{\infty} (-1)^n \frac{\lambda_n^2 a_n}{D} = -R_A + R_E|_{x=-1}, \end{cases} \end{aligned}$$

where we used the properties

$$\frac{d\phi_n(1)}{dx} = \frac{\lambda_n}{2} \quad \text{and} \quad \phi_n(-x) = (-1)^n \phi_n(x).$$

## 1.2 Discretisation

We choose to decompose the temperature field into a sum of orthogonal Legendre polynomials, i.e.

$$T(x) = \sum_{n=0}^{\infty} a_n \phi_n(x),$$

where the timedependence is dropped seeing as we are after equilibrium solutions.

Subsitution of the above in the (equilibrium) energy balance equation yields

$$-\sum_{i=0}^{\infty} \frac{\lambda_i a_i}{D} \phi_i + R_A(T, x) + R_E(T) = 0.$$

We now use Galerkin's method to project the above equation onto the Legendre basis functions. This gives

$$F_i(T(\mathbf{a})) = \int_{-1}^1 \left[ -\sum_{i=0}^{\infty} \frac{\lambda_i a_i}{D} \phi_i + R_A(T, x) + R_E(T) \right] \phi_i dx = 0.$$

where  $F_i$  is the  $i$ th component of discretised equilibrium energy balance eqaution. Hence the above defines a non-linear system of equations. Note that we could have used the orthogonality of the Legendre polynomials to simplify the above, but we chose to keep the above form for clarity. Moreover, letting  $n_p$  be the number of legendre polynomials we can approximately evaluate the above (and coming) integral(s) using the Gauss-Legendre quadrature rule with  $2n_p$  quadrature points.

## 1.3 Derivation: exact vs. numerical

We want the jacobian of the non-linear system  $\mathbf{F}_T = \frac{\partial F(T(\mathbf{a}))}{\partial \mathbf{a}}$ , which we may obtain directly from the previous secttion using the same Galerkin method and guassian quadrature

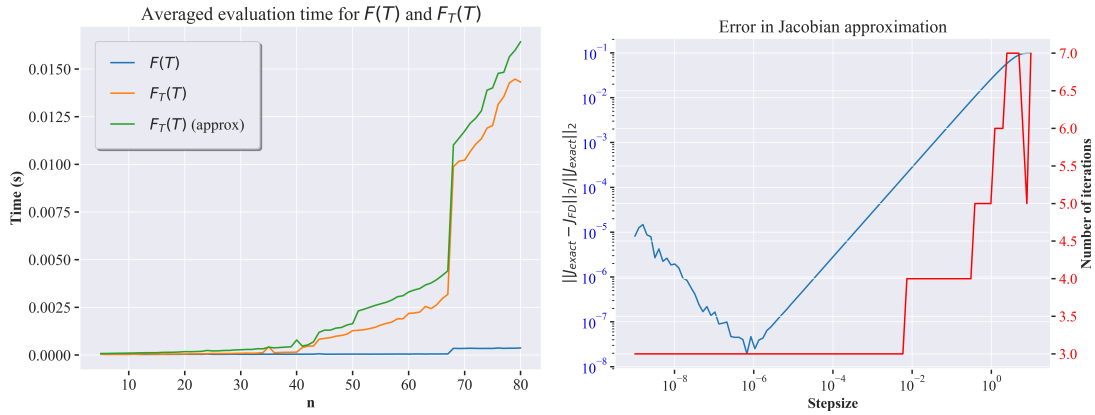
$$\frac{\partial F_i}{\partial a_j} \approx \int_{-1}^1 \left[ -\frac{\lambda_i}{D} + \frac{\partial R_A(T, x)}{\partial T} + \frac{dR_E(T)}{dT} \right] \phi_j \phi_i dx = 0. \quad (1)$$

Alternatively, we can use the finite difference method to approximate the jacobian.

$$\frac{\partial F_i}{\partial a_j} = \frac{F_i(T(\mathbf{a} + h\mathbf{e}_j)) - F_i(T(\mathbf{a}))}{h} + \mathcal{O}(h). \quad (2)$$

Both methods are approximations. However, the finite difference method is fundamentally an approximation of order  $h$ , whereas Galerkin is exact up to order  $n_p$ . With regards to computational cost the finite difference method requires  $n_p$  evaluations of the non-linear system, whereas the Galerkin method requires  $n_p^2$  numerical integrations of the derivative of the non-linear system. Hence for relatively small  $n_p$ , the Galerkin method is preferable. Since the non-linear system is not too complex, we can afford to use the Galerkin method.

With regards to computational complexity and accuracy we refer to Figures 1a and 1b. The former compares the computational time for one evaluation of the non-linear system as well as the jacobian using both the Galerkin and finite difference methods. The latter compares the correspondence between the two jacobians for different values of  $h$ .



(a) Computational time for one evaluation of the non-linear system and the jacobian using both the Galerkin and finite difference methods. (b) Comparison of the jacobian obtained using the Galerkin and finite difference methods for different values of  $h$ .

**Figure 1:** Comparison of the Galerkin and finite difference methods.

As explained during the lectures, there exists an optimal value of  $h$  for which the finite difference method is most accurate. From the 1b we see that the finite difference method is most accurate for  $h \approx 10^{-6}$ . However, we also see from 1a that the computational time for the finite difference method is comparable to the Galerkin method for problem sizes with  $n_p \leq 80$ . This means that as far as this assignment is concerned, the Galerkin method is preferable.

## 1.4 Finding equilibria: Newton and Broyden

Figure 2 shows the equilibria found using the Newton and Broyden methods.

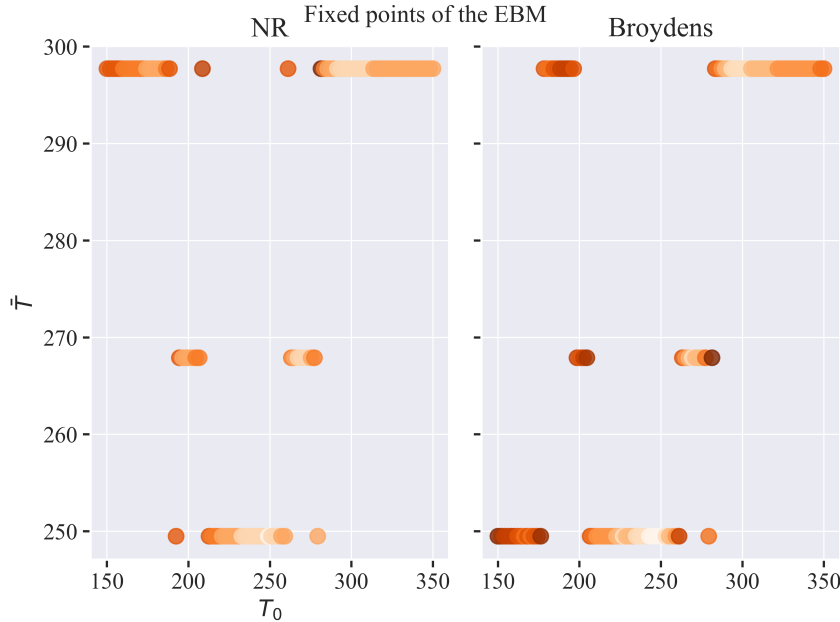


**Figure 2:** Equilibria found using the Newton and Broyden methods for a range of homogeneous initial temperatures  $T_0$ . The color intensity indicates the amount of iterations required to converge. A high intensity indicates the method needed a low amount of iterations to converge.

We notice that roughly speaking the equilibria found using the Newton and Broyden methods are the same. However, the Broyden method seems to be less predictable in terms of what root it converges. It is not directly clear how to compare domains of attraction for these two methods. However, we can see that the Newton method is more predictable in terms of the number of iterations required to converge and what initial state ends up converging to what root. In other words, the Broyden method seems to be more sensitive to the initial state. This might be due to the fact that the Broyden method's linear compared to Newton method's quadratic convergence rate causes it to 'skip' roots.

In terms of the state of our model Earth, we discover three distinct average temperatures  $T_{eq} \approx 250K$ ,  $T_{eq} \approx 268K$  and  $T_{eq} \approx 298K$ . The first corresponds to a frozen Earth, the second to a partially frozen Water world and the third to quite a cozy Blue Marble.

## 1.5 Embedding

We can reduce the problem of finding the first equilibrium through the following embedding of the energy balance equation

$$f = \gamma R_D[T] + (1 - \gamma)(R_A(T, x) + R_E(T)). \quad (3)$$

Taking  $\gamma = 0$  we obtain a transcendental equation for the equilibrium temperature, which we can easily solve using the Newton method. Once we have this solution we increment  $\gamma$  and apply some continuation scheme using the methods for evaluating the non-linear system and its jacobian. This way we can find the other equilibria. We repeat this until we reach  $\gamma = 1$ , at which point we find an initial equilibrium.

## 1.6 Bifurcation diagrams

The pseudo arclength continuation is implemented by first introducing the parametrisation  $(T, \mu) \mapsto (T(s), \mu(s))$ . This results in an extended system of equations, which is the original

system with an additional parametrisation equation.

$$\begin{cases} F(T(s), \mu(s)) = 0, \\ p(T, \mu, s) = 0. \end{cases},$$

where

$$p(T, \mu, s) = 2\zeta(T - \bar{T}) \frac{dT}{ds} + 2(1 - \zeta)(\mu - \bar{\mu}) \frac{d\mu}{ds} - \Delta s,$$

where  $(\bar{T}, \bar{\mu})$  denote the current equilibrium,  $(T, \mu)$  the continued (as of yet unknown) solution,  $\zeta$  is a tune factor and  $\Delta s$  is the arclength or step size

The jacobian of this system is given by

$$\tilde{F}' = \begin{bmatrix} \frac{\partial F}{\partial T} & \frac{\partial F}{\partial \mu} \\ \frac{\partial p}{\partial T} & \frac{\partial p}{\partial \mu} \end{bmatrix},$$

which after discretisation becomes

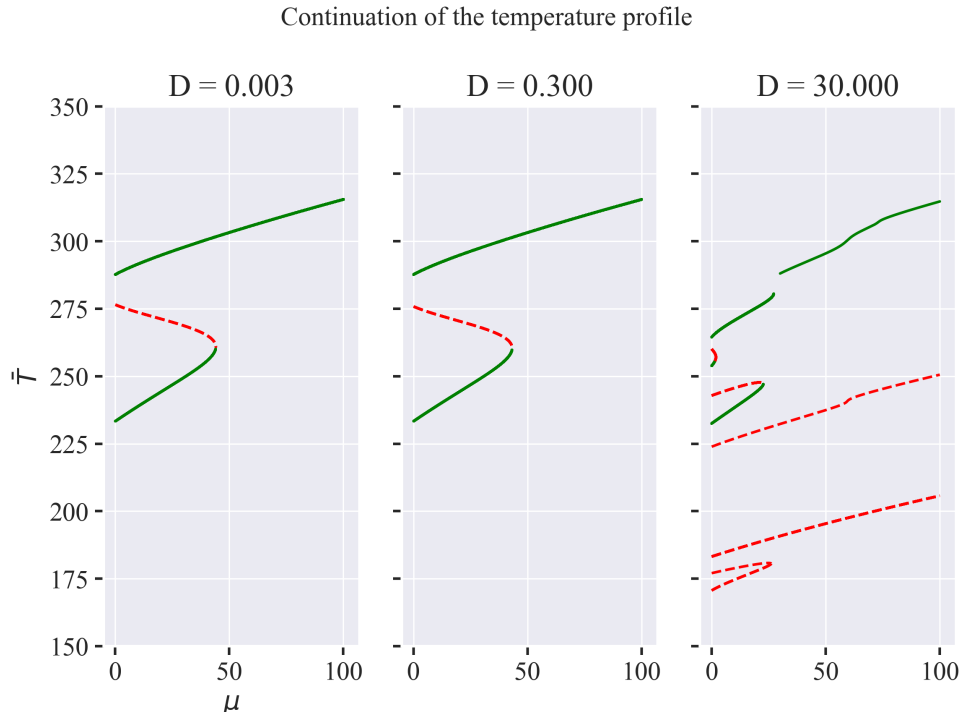
$$D\tilde{F} = \begin{bmatrix} \frac{\partial \mathbf{F}}{\partial \mathbf{a}} & \frac{\partial \mathbf{F}}{\partial \mu} \\ 2\zeta \left(\frac{d\mathbf{T}}{ds}\right)^T & 2(1 - \zeta) \frac{d\mu}{ds} \end{bmatrix}.$$

The above system can be solved using the Newton method. The condition for convergence is such that the update

$$\begin{bmatrix} \Delta \mathbf{a} \\ \Delta \mu \end{bmatrix} = - (D\tilde{F})^{-1} \begin{bmatrix} \mathbf{F} \\ p \end{bmatrix},$$

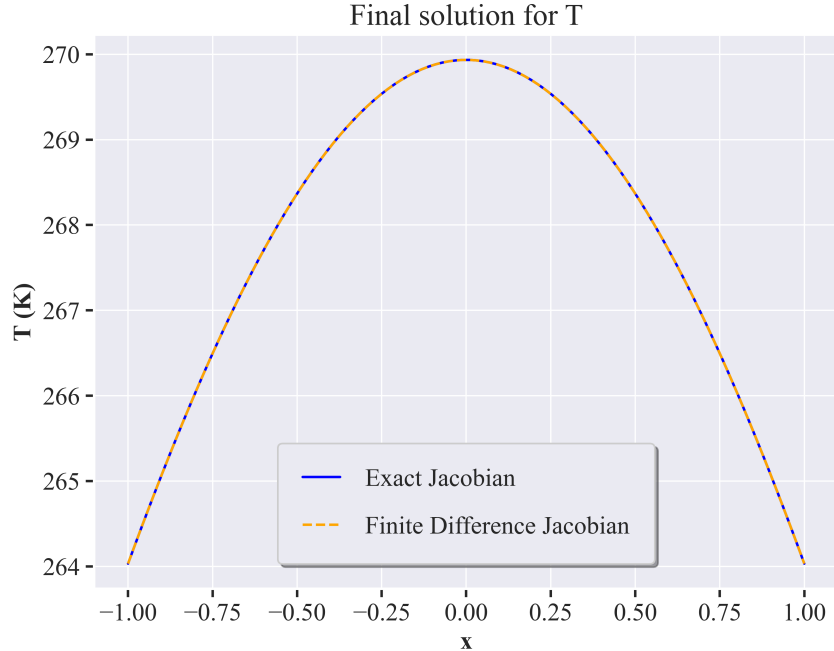
must be smaller than some tolerance  $\epsilon = 10^{-5}$ .

Figure 3 shows the bifurcation diagram for the Earth model. This figure was made by rerunning the continuation scheme for different initial temperatures  $T_0$  and plotting the equilibria found.



**Figure 3:** Bifurcation diagram for the Earth model. Green solid lines indicates a stable branch while red, dashed lines indicate an unstable branch.

A typical temperature profile is given in Figure 4. We see that the temperature profile is symmetric around the equator, which is expected.



**Figure 4:** Typical temperature profile for the Earth model.

We see from Figure 3 that we need a small step size to accurately resolve all the branches in the bifurcation diagram ( $\Delta s \leq 0.1$ ). Additionally, we should place emphasis on tracking small changes in the parameter ( $\zeta \leq 0.001$ ).

In figure 3 we solely identify fold (subtle) and jump (critical) bifurcations.

Next to this we recover the three equilibria found above. For small values of the diffusion constant  $D = 0.003, 0.3$  we find that for  $\mu \gtrapprox 50$  there is only one stable branch. In case of the partially frozen Earth, we see that increasing  $\mu$  at first has the effect of lowering the temperature. However, at some point it appears the greenhouse effect becomes strong enough to counteract the cooling effect of the ice the solution suddenly jumps to the aforementioned stable branch.

This behaviour is radically different however for  $D = 30$ . We suddenly see many more branches appearing. This is due to the fact that the heat dispersion is so strong that the temperature gradient is much steeper. This results in initially completely ice covered earths to become unstable.

## 1.7 Conclusion

We have found the equilibria of the Earth model and studied the bifurcation diagram. We have seen that for default parameter values the Earth model has three distinct equilibria, corresponding to a frozen, a partially frozen and a warm Earth. We have also seen that the bifurcation diagram is sensitive to the diffusion constant  $D$ . For small values of  $D$  we see that the bifurcation diagram is relatively simple, with only fold and jump bifurcations. However, for large values of  $D$  the bifurcation diagram becomes much more complex, with many more branches appearing. This is due to the fact that the heat dispersion is so strong that the temperature gradient is much steeper. This results in initially completely ice covered earths to become unstable.

## Assignment 2

In this assignment we study the MCM system of equations, which models the interaction between three species of cells, tumor-, healthy- and effector cells. The corresponding system of equations is given by

$$\begin{aligned} T' &= r_1 T \left(1 - \frac{T}{k_1}\right) - a_{12} TH - a_{13} TE, \\ H' &= r_2 H \left(1 - \frac{H}{k_2}\right) - a_{21} TH, \\ E' &= \frac{r_3 TE}{T + k_3} - a_{31} TE - d_3 E, \end{aligned}$$

and its dimensionless form

$$\begin{aligned} x'_1 &= x_1 (1 - x_1) - p_1 x_1 x_2 - p_2 x_1 x_3, \\ x'_2 &= p_3 x_2 (1 - x_2) - p_4 x_1 x_2, \\ x'_3 &= \frac{p_5 x_1 x_3}{x_1 + p_6} - p_7 x_1 x_3 - p_8 x_3. \end{aligned}$$

The parameters  $p_i$  are specified in Table 2

Parameter	Definition	description	Value
$p_1$	$\frac{a_{12}k_2}{r_1}$	T->H competition	0.5
$p_2$	$\frac{a_{31}k_1}{r_1}$	E->T killing	2.5
$p_3$	$\frac{r_2}{r_1}$	H-T growth ratio	0.6
$p_4$	$\frac{a_{21}k_1}{r_1}$	T->H inactivation	1.5
$p_5$	$\frac{r_3k_2}{r_1}$	T->E stimulation	4.5
$p_6$	$\frac{k_3}{k_1}$	E-T capacity ratio	1.0
$p_7$	$\frac{a_{31}k_3}{r_1}$	T->E inactivation	0.2
$p_8$	$\frac{d_3}{r_1}$	E natural death	0.5

**Table 2:** Parameters of the dimensionless system

The goal of this assignment is to study the dynamics of this system as the parameter  $p_1$  is varied. We aim to find the stationary points, bifurcations and (stable) limit cycles of the system, and study their stability.

Additionally, we aim to find the period doubling bifurcations of the limit cycles, and study the stability of the resulting period-doubled limit cycles. Eventually, we aim to determine the period doubling route to chaos.

### 2.1 Stationary points

Table 3 shows the stationary points of the system.

index	$x_1$	$x_2$	$x_3$	stability
1	-2.00	6.00	0.00	Unstable
2	0.00	0.00	0.00	Unstable
3	0.00	1.00	0.00	Unstable
4	$1.33 \times 10^{-1}$	0.00	$3.47 \times 10^{-1}$	Unstable
5	$1.33 \times 10^{-1}$	$6.69 \times 10^{-1}$	$2.13 \times 10^{-1}$	Stable
6	1.00	0.00	0.00	Unstable
7	$1.89 \times 10^1$	$-4.62 \times 10^1$	2.09	Unstable
8	$1.89 \times 10^1$	0.00	-7.15	Stable

**Table 3:** Stationary points of the MCM model.

## 2.2 Continuation of stationary points

We observe two stable stationary points (indices 5 and 8). We continue these points in the parameter  $p_1 \in [0.5, 1]$  and plot the continuation in Figure 5.

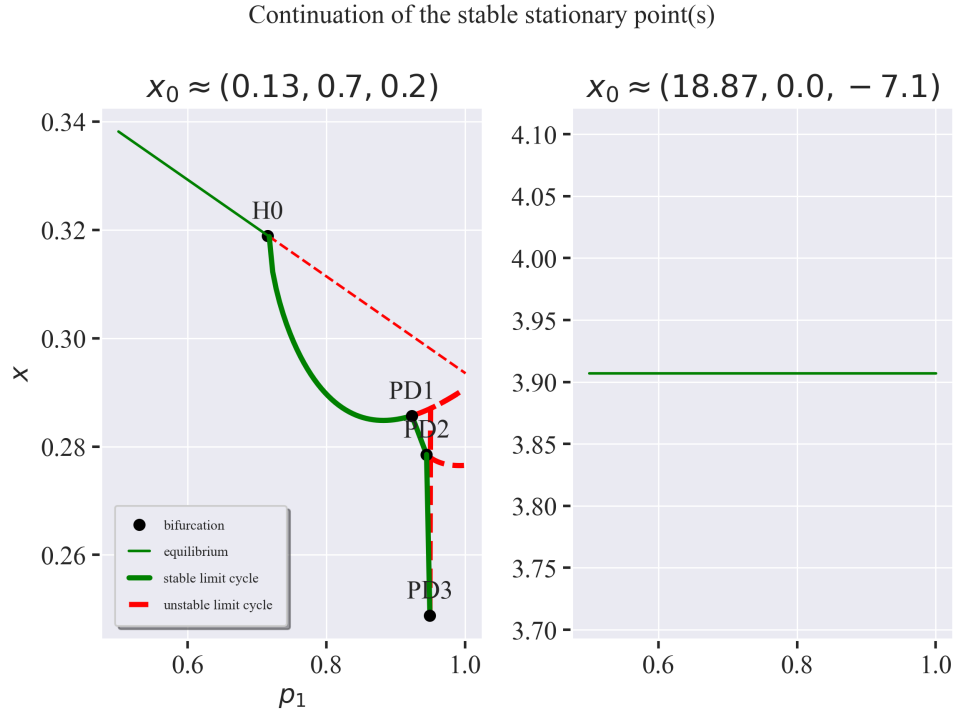


**Figure 5:** Continuation using the arc-length method of the stable stationary points in the parameter  $p_1$ , point 5 (left) and point 8 (right). The former encounters a bifurcation at  $p_1 \approx 0.71$ . From this Hopf-bifurcation (**H0**) an unstable stationary solution and a stable limit cycle emerges. This limit cycle then encounters a period doubling bifurcation at  $p_1 \approx 0.923$  (**PD1**) and splits into a stable and unstable part. The stable part then encounters another period doubling bifurcation at  $p_1 \approx 0.944$  (**PD2**) and splits again. The stable part of this limit cycle then encounters a third period doubling bifurcation at  $p_1 \approx 0.949$  (**PD3**). However, the last bifurcation is not stable and the limit cycle seems to rejoin the original limit cycle.

The bifurcation that occurs during the continuation of point 5 in Figure 5 is given by

**Bifurcation type :** Hopf  
**Label :** H0  
**Parameter :**  $p_1$   
**Critical value :** 0.71  
**Eigenvalues :**  $0 \pm 0.36i, -0.53$   
**x :** 0.13, 0.67, 0.16

This bifurcation point was found by applying an indirect method based on the interpolation of test function values, adapted from Seydel's book (section 5.3.1). The particular test function used was the maximum of the real part of the eigenvalues of the system Jacobian.

The bifurcation is a Hopf-bifurcation, as a complex pair of eigenvalues crosses the imaginary axis with non-zero velocity. That is to say, the eigenvalues of the system jacobian at the continuation step directly before and after the bifurcation are

$$\begin{array}{ll} \text{before:} & -1.4 \times 10^{-4} \pm 0.36i, -0.53, \\ \text{after:} & 1.38 \times 10^{-4} \pm 0.36i, -0.53 \end{array}$$

which shows the eigenvalues pass the imaginary axis with non-zero velocity.

From the (static) Hopf-bifurcation we determine the first dynamical solution using the method described in section 7.6.2 of Seydel's book. In other words we solve the following BVP

$$\begin{pmatrix} \mathbf{x} \\ T \\ \lambda \\ \mathbf{h} \end{pmatrix}' = \begin{pmatrix} T\mathbf{f}(\mathbf{x}, \lambda) \\ 0 \\ 0 \\ T\mathbf{f}_x(\mathbf{x}, \lambda)\mathbf{h} \end{pmatrix}, \quad \begin{pmatrix} \mathbf{x}(0) - \mathbf{x}(1) \\ \mathbf{h}(0) - \mathbf{h}(1) \\ \sum_i h_i \partial f_i / \partial x_i \\ h_1(0) - 1 \end{pmatrix} = \mathbf{0}, \quad (4)$$

using the shooting method in order to switch from the stationary solution to the limit cycle. In particular, we initialize the system to a point either on or close to the Hopf-bifurcation, because this point is close to the limit cycle. We then provide an initial guess for the period of the limit cycle, and solve the BVP using the shooting method. To do so, we make use of Scipy's `integrate.solve_ivp` and `optimize.fsolve` functions. In short, the former allows us to integrate the system of ODEs, while the latter allows us to solve the BVP.

Going into more detail, we use `integrate.solve_ivp`<sup>1</sup> to integrate the system of ODEs over some period  $T$  and then use the final values of the integration to calculate the residuals of the boundary conditions. This defines an objective function that we want to minimize. We then use `optimize.fsolve` to find the values of the initial conditions that make the residuals zero. `optimize.fsolve` will effectively find the initial conditions that make the solution of the BVP a limit cycle.

The solution we obtain upon completing above process is

$$\begin{aligned} \mathbf{x}^{(0)} &= (0.13, 0.67, 0.15) \\ T^{(0)} &= 17.6 \\ p_1^{(0)} &= 0.72 \\ \mathbf{h}^{(0)} &= (1.00, -1.40, 0.00), \end{aligned}$$

from which we get a more accurate estimate for the period of the limit cycle.

---

<sup>1</sup>We use a maximum timestep of 0.001. I did not do initially and it gave the wrong results I discussed in my last submission. Same goes for the Floquet multipliers, for which I used the same Scipy function. Fixing the max time step now gives the right values allowing me to find the period doubling bifurcations.

### 2.3 Continuation of limit cycle from Hopf-bifurcation

We use the solution of the BVP from the previous section as an initial guess for the continuation of the limit cycle. Following the method outlined in section 7.6.3 of Seydel's book, we continue the limit cycles from the dynamic Hopf-bifurcation point  $(\mathbf{x}^{(0)}, T^{(0)}, p_1^{(0)}, \mathbf{h}^{(0)})$  in the parameter  $p_1$  by repeatedly solving the boundary value problem (Seydel, Equation 7.6c, p. 306)

$$\begin{pmatrix} \mathbf{x} \\ T \\ \lambda \end{pmatrix}' = \begin{pmatrix} Tf(\mathbf{x}, \lambda) \\ 0 \\ 0 \end{pmatrix}, \quad \begin{pmatrix} \mathbf{x}(0) - \mathbf{y}(1) \\ f_j(\mathbf{y}(0), \lambda) \\ p_1^{(k+1)} - p_1^{(k)} - \delta_p \end{pmatrix} = \mathbf{0}, \quad (5)$$

where  $\delta_p \approx 0.005$  is a small value that determines the step size in the parameter  $p_1$  and  $j = 1$  (phase condition).

The shooting method needs an initial guess, as it is really just a root finding algorithm. Therefore, each iteration starts with the solution of the previous iteration. Note that the first iteration starts with a small perturbation in the direction of  $\mathbf{h}$  (Equation 7.24, Seydel)

$$\text{initial guess: } \mathbf{x}^{(k+1)} = \begin{cases} \mathbf{x}^{(0)} + \delta_h \mathbf{h}^{(0)}, & \text{if } k = 0, \\ \mathbf{x}^{(k)}, & \text{otherwise,} \end{cases} \quad T^{(k+1)} = T^{(k)}, \quad p_1^{(k+1)} = p_1^{(k)},$$

for a suitably small parameter  $\delta_h \approx 0.01$ . This results in a sequence of limit cycles starting from the Hopf point ( $k=0$ )

$$\text{cycle}^{(k)} = \left\{ \mathbf{x}^{(k)}, T^{(k)}, p_1^{(k)} \right\}, \quad k = 0, 1, 2, \dots$$

which we integrate over their respective periods and plot in Figure 6.

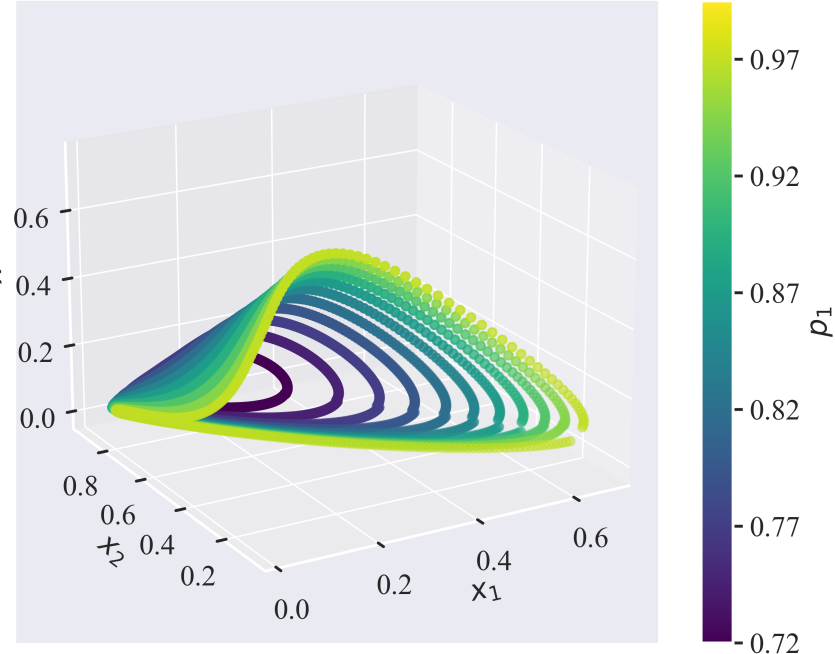


**Figure 6:** Continuation of the limit cycle in the parameter  $p_1$ . The colors indicate the increase in  $p_1$  from dark to light.

The limit cycles in Figure 6 are averaged both in time and in space to obtain the points in Figure 6; thick green line from **H0** to **PD1** and thick, dashed red line from **PD1** to the end of the graph.

For each limit cycle we calculate the monodromy matrix  $M$  using Algorithm 7.12 from section 7.5.1 of Seydel. The eigenvalues of  $M$  (Floquet multipliers)  $\mu_j$  are then used to determine the stability of the limit cycle (according to Summary 7.5, p. 315, Seydel).

The stability of the limit cycles obtained from this process is accordingly shown in Figure 5, where the thick green- and thick, dashed red lines indicate stable and unstable limit cycles, respectively.

## 2.4 Period doubling bifurcations

Period doubling bifurcations occur at those limit cycles where there is a  $j$  for which  $\mu_j = -1$ . Hence, we continue the limit cycle (and calculate the monodromy matrices) until we find a multiplier close to  $-1$ .<sup>2</sup> We then use interpolation to find the exact value of  $p_1$  at which the period doubling bifurcation occurs. Doing this for the limit cycle we discussed in the previous section we find the **first period doubling bifurcation**:

**Bifurcation type** : period doubling  
**Label** : PD1  
**Parameter** :  $p_1$   
**Critical value** : 0.923  
**Floquet multipliers** :  $-1.00, 0, 1.00 \leftarrow$  note the -1  
 $\mathbf{x} = (0.59, 0.17, 0.10)$   
**Period** : 31.55

Starting from this interpolated period doubling bifurcation point we apply the shooting method to solve the BVP in Equation 7.27 of Seydel's book.

$$\begin{pmatrix} \mathbf{x} \\ T \\ \lambda \\ \mathbf{h} \end{pmatrix}' = \begin{pmatrix} T\mathbf{f}(\mathbf{x}, \lambda) \\ 0 \\ 0 \\ T\mathbf{f}_x(\mathbf{x}, \lambda)\mathbf{h} \end{pmatrix}, \quad \begin{pmatrix} \mathbf{x}(0) - \mathbf{x}(1) \\ p(\mathbf{x}(0), \lambda) \\ \mathbf{h}(0) + \mathbf{h}(1) \\ h_k(0) - 1 \end{pmatrix} = 0. \quad (6)$$

This gives a point on the period doubled branch  $(\mathbf{x}^{(0)}, T^{(0)}, p_1^{(0)}, \mathbf{h}^{(0)})$ , which we can continue in the same way as we did in the previous section. That is to say, we repeatedly apply the shooting method to BVP in Equation 5. The only differences being that we take slightly smaller steps  $\delta_p = 0.001$ , and we specify slightly different initial guesses for the continuation of the period-doubled limit cycle. Namely,

$$\begin{aligned} \text{initial guess: } \mathbf{x}^{(k+1)} &= \begin{cases} \mathbf{x}^{(0)} + \delta \mathbf{h}^{(0)}, & \text{if } k = 0, \\ \mathbf{x}^{(k)}, & \text{otherwise,} \end{cases} \\ T^{(k+1)} &= \begin{cases} 2T^{(0)}, & \text{if } k = 0, \\ T^{(k)}, & \text{otherwise,} \end{cases} \\ p_1^{(k+1)} &= p_1^{(k)}. \end{aligned}$$

This results in Figure 7 where we plot the period-doubled limit cycles in the parameter  $p_1$ .

---

<sup>2</sup>We use a tolerance of 0.01.

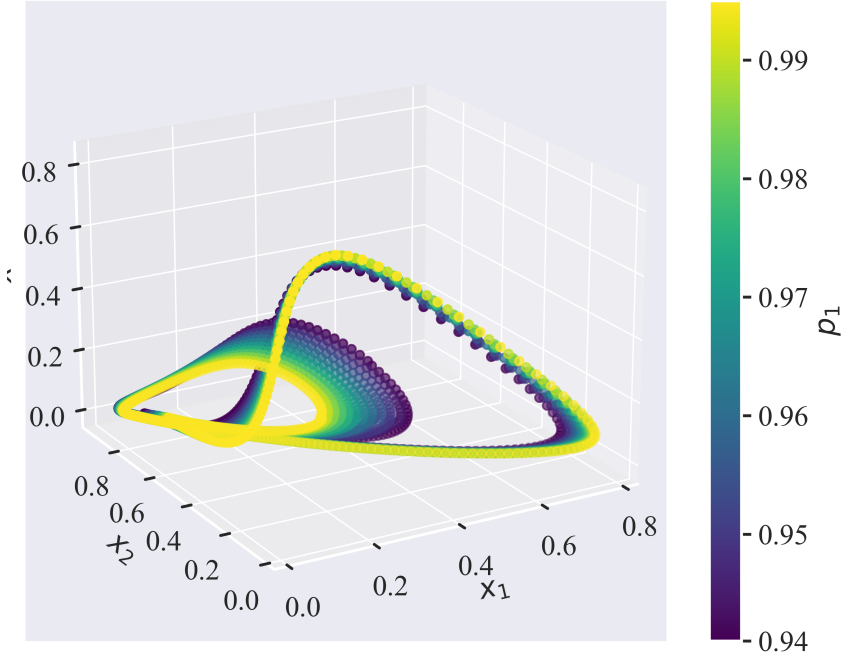


**Figure 7:** Similar to Figure 6, but now showing the period-doubled limit cycles. Note the double loop in the limit cycle.

By again calculating the monodromy matrix and corresponding Floquet multipliers for every cycle, we find the second period-doubling bifurcation

**Bifurcation type** : period doubling  
**Label** : PD2  
**Parameter** :  $p_1$   
**Critical value** : 0.944  
**Floquet multipliers** :  $-1.00, 0, 1.00$   
 $\mathbf{x} = (0.43, 0.28, 0.12)$   
**Period** : 64.92

We can continue the steps outlined above to find more period-doubling bifurcations. For instance, the third period-doubling bifurcation occurs at

**Bifurcation type** : period doubling  
**Label** : PD3  
**Parameter** :  $p_1$   
**Critical value** : 0.949  
**Floquet multipliers** :  $-1.00, 0, 1.00$   
 $\mathbf{x} = (0.47, 0.19, 0.09)$   
**Period** : 130.3

However, this result must be taken with a grain of salt, as the remaining branch this bifurcation is unstable and seems to rejoin the original limit cycle stemming from the Hopf bifurcation for  $p_1 > 0.949$ .

As an alternative, we can predict the parameter values at which we expect period-doublings to occur using Feigenbaum's law (Equation 7.14, Seydel)

$$\lim_{n \rightarrow \infty} \frac{p_{n+1} - p_n}{p_n - p_{n-1}} = 0.21416 \dots, \quad (7)$$

This gives the following predictions for the period-doubling bifurcations in Table 4.

## 2.5 Route to chaos

In order to determine whether a system exhibits chaos, we (numerically) calculate the Lyapunov exponents of the system. We use the above predicted values for the period-doubling bifurcations as well as the point **PD3** as an initial condition. Then we iteratively integrate the system over a large time-span ( $t_{\text{end}} = 100$ ) with small timestep ( $dt = 0.001$ ) and calculate the Lyapunov exponents at each iteration. The Lyapunov exponents are then averaged over time to obtain the approximate Lyapunov spectrum.<sup>3</sup>

Period doubling	$p_1$	Lyapunov spectrum
PD1	<b>0.923</b>	0.00, -0.04, -0.50
PD2	<b>0.944</b>	0.01, -0.06, -0.51
PD3	0.949	0.02, -0.06, -0.52
PD4	0.950	0.02, -0.06, -0.52
PD5	0.950	0.02, -0.06, -0.52
PD6	0.950	0.02, -0.06, -0.52

**Table 4:** Predicted period doubling bifurcations using Feigenbaum's law and corresponding approximated Lyapunov exponents. **PD1** and **PD2** are taken from the continuation of the limit cycles, while the rest are predicted using the recurrence relation in Equation 7.

We observe that one Lyapunov exponent is positive for values of  $p_1 > 0.944$ . This indicates that the system is chaotic for these values of  $p_1$ .

## 2.6 Conclusion

In the above treatment of the MCM system we

1. Found the stationary points of the system and continued the stable ones in the parameter  $p_1$ ;
2. Found a Hopf-bifurcation at  $p_1 \approx 0.71$  and calculated the first limit cycle using the shooting method;
3. Continued the limit cycle in the parameter  $p_1$  and calculated the stability of the limit cycles;
4. Found the first, second and third period-doubling bifurcations at  $p_1 \approx 0.923$ ,  $p_1 \approx 0.944$  and  $p_1 \approx 0.949$ , respectively;
5. Verified the period-doubling bifurcations using Feigenbaum's law and calculated the Lyapunov exponents of the system;
6. Determined that the system exhibits chaos for  $p_1 > 0.949$ .

---

<sup>3</sup>this algorithm is adapted from [CHAOS: An Introduction to Dynamical Systems](#) by Kathleen Alligood, section 5.2 "Numerical Calculation of Lyapunov Exponents", p.199 (214 in pdf).

## Assignment 3

### 3.1 Introduction

In this assignment, we will study the behavior of a system of ordinary differential equations that models the dynamics of a cell, also known as ‘cell motility’. The system is given by

$$\begin{cases} \hat{R}'_a &= \frac{\hat{A}(1-\hat{R}_a)}{\hat{\rho}_a^n + \hat{\rho}_0^n} - \hat{\delta}_R \hat{R}_a \\ \hat{\rho}'_a &= \frac{\hat{B}(1-\hat{\rho}_a)}{\hat{R}_0^n + \hat{R}_a^n} - \hat{\delta}_a \end{cases} \quad (8)$$

As stated in the assignment, the goal here is to: ‘to investigate the effect of changes in the parameter  $\hat{B}$  due to external stimuli. Focus is on comparing the model behavior under quasi-stationary and time-dependent parameter variations’

### 3.2 Autonomous system

Figure 8 shows the continuation of the system with the following parameters (default):  $R_0 = 0.3$ ,  $\rho_0 = 0.16$ ,  $\delta R = 1$ ,  $n = 4$ ,  $B_{max} = 0.04$  and  $\epsilon = 0.0$ .

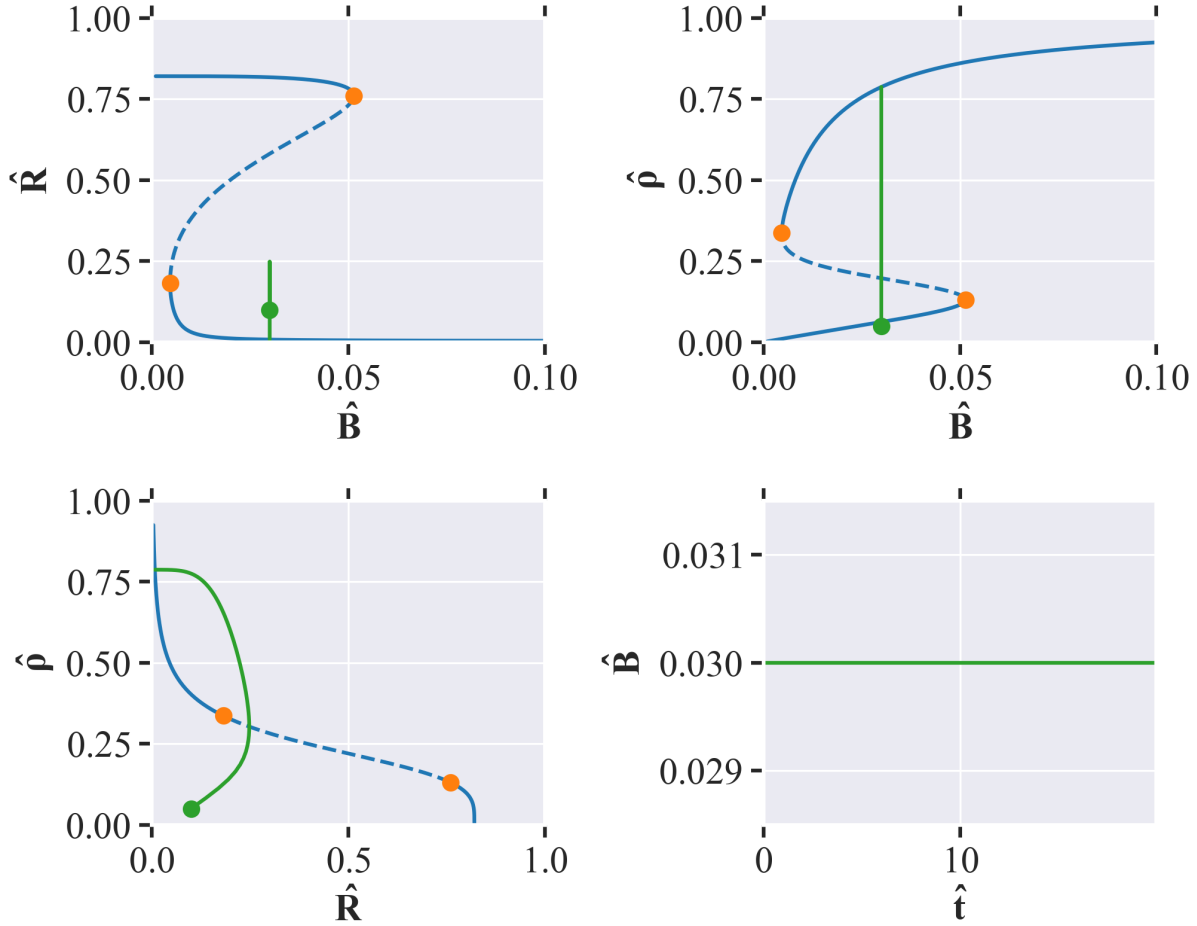


**Figure 8:** Figure of the continuation of **top left:**  $(\hat{R}, \hat{B})$  and **top right:**  $(\hat{\rho}, \hat{B})$ , **bottom left:** phase space  $(\hat{\rho}, \hat{R})$  and **bottom right:**  $\hat{B}$  against time (time horizon of 20 seconds with a time step of 0.01). Dots (orange) indicate turning points.

The system is at this stage effectively autonomous, since  $\hat{B}(\hat{t}) \equiv \hat{B}_c$  is taken to be constant. Continuation is subsequently done with respect to the parameter  $\hat{B}$ . We observe two turning point bifurcations at:

$$1. \hat{B} \approx 0.051, \hat{R} \approx 0.759, \hat{\rho} \approx 0.131;$$

$$2. \hat{B} \approx 0.005, \hat{R} \approx 0.182, \hat{\rho} \approx 0.337.$$

Using the graph to get initial guesses for our Newton root finding method, we find there exist three equilibrium:

$$E_0 = (\hat{R}_a, \hat{\rho}_a) \approx (0.58, 0.20) \leftarrow \|E_0\| \approx 0.61,$$

$$E_1 = (\hat{R}_a, \hat{\rho}_a) \approx (0.01, 0.79) \leftarrow \|E_1\| \approx 0.79,$$

$$E_2 = (\hat{R}_a, \hat{\rho}_a) \approx (0.82, 0.06) \leftarrow \|E_2\| \approx 0.82.$$

$E_0$  is unstable, while  $E_1$  and  $E_2$  are stable. Moreover, looking at the trajectory in the phase space  $(\hat{\rho}, \hat{R})$ , we see that the system converges to  $E_1$ . Therefore,  $E_1$  is the attractor in this case.

In figure 9 the domains of attraction of  $E_i$ ,  $i = 1, 2, 3$  are shown.

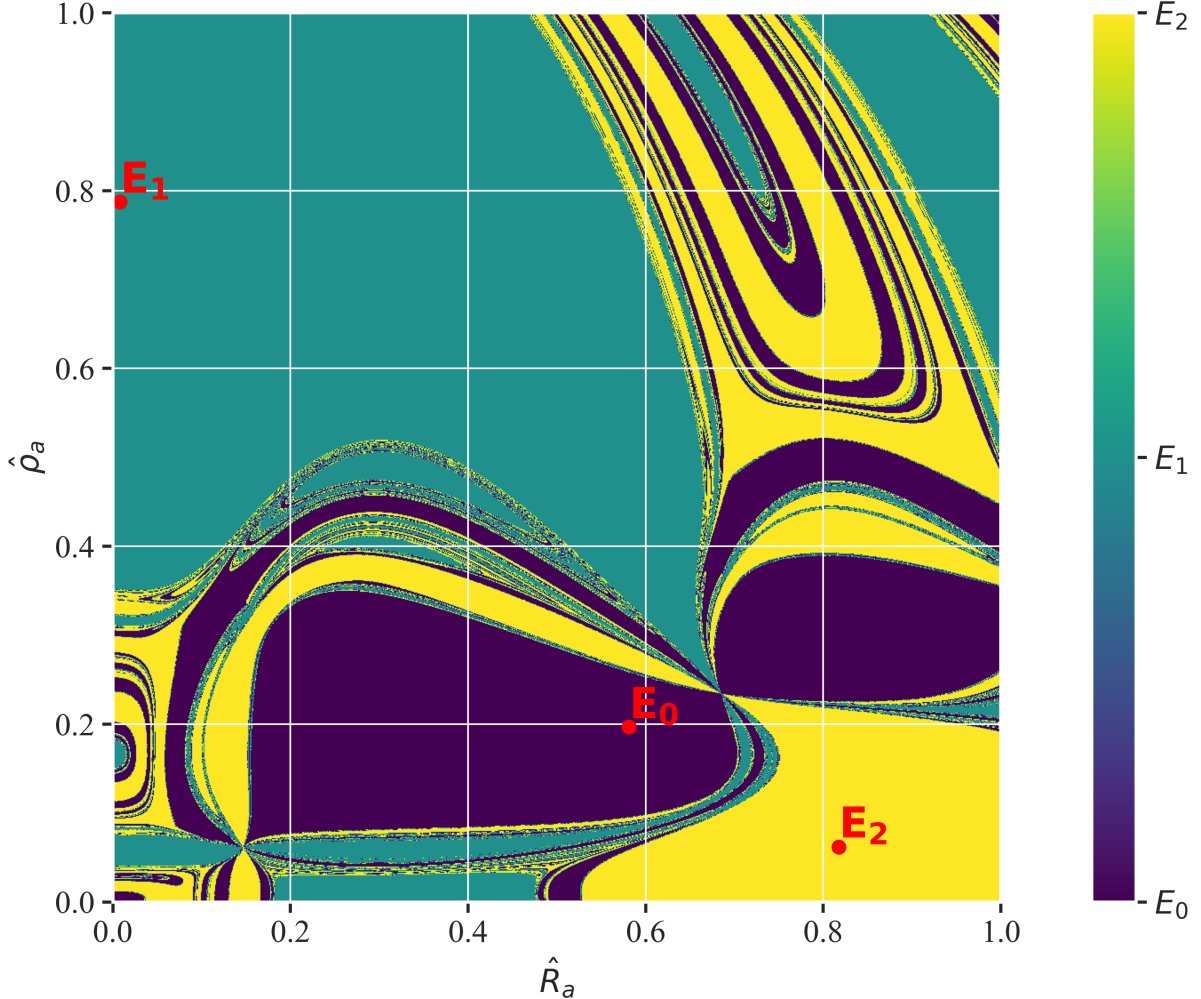


**Figure 9:** Domains of attraction of  $E_i$ ,  $i = 1, 2, 3$ . The color of a certain area in the plot indicates which equilibrium point the system converges to (purple to  $E_0$ , yellow to  $E_1$  and cyan to  $E_2$ ). This is done by performing a Newton root finding method on a grid of initial conditions in the phase space  $(\hat{\rho}, \hat{R})$ . The red dots indicate the equilibrium points themselves. Close to the equilibrium points, the system converges to the equilibrium point itself, in keeping with the theory on Newton(-like) methods. However, further away from the equilibrium points, we get an amazingly complex mixture of the various domains of attractions. Looks like someone folded hyperspace in on itself and slapped it flat, so we could see it.

### 3.3 Non-autonomous system

We now introduce a ‘small’ linear time-dependent perturbation to  $\hat{B}$ . That is, the perturbed system is now given by

$$\begin{cases} \hat{R}'_a &= \frac{\hat{A}(1-\hat{R}_a)}{\hat{\rho}_a^n + \rho_0^n} - \hat{\delta}_R \hat{R}_a \\ \hat{\rho}'_a &= \frac{\hat{B}(1-\hat{\rho}_a)}{\hat{R}_0^n + \hat{R}_a^n} - \hat{\rho}_a \\ \hat{B}' &= \epsilon, \end{cases} \quad (9)$$

where  $\epsilon$  is small or big with respect to the linearized system dynamics (reciprocal of the linearized system’s eigenvalues).

Figures 10 and 11 show the continuation of the autonomous system, as well as a trajectory of the system for  $\epsilon = 0.0001$  and  $\epsilon = 0.01$  respectively. For small  $\epsilon$ , the system has sufficient time to restore to its autonomous (quasi-)equilibrium. This is no longer the case for big  $\epsilon$ .

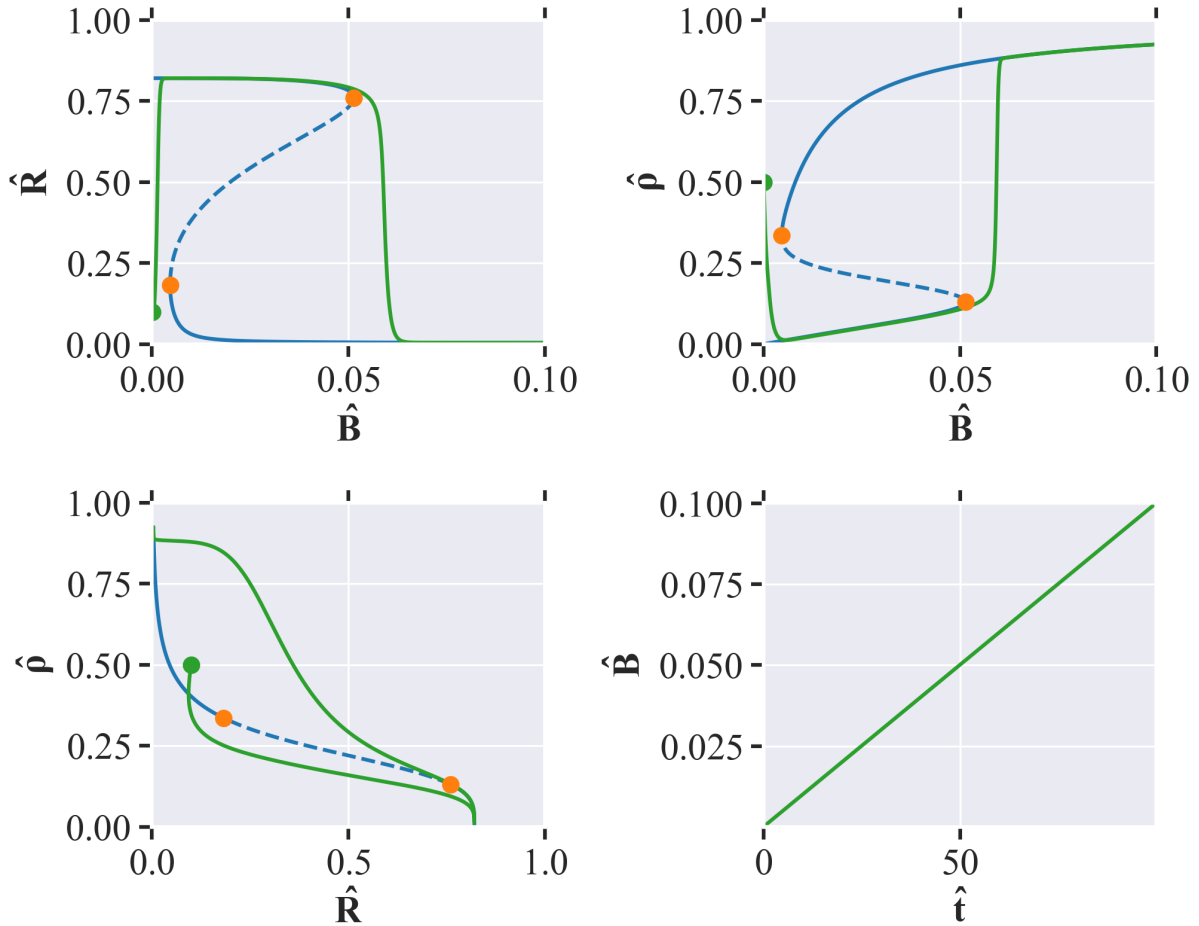


**Figure 10:** System behavior for small  $\epsilon = 0.0001$ . Plotted are the unperturbed system’s equilibria and a trajectory of the perturbed system with initial condition  $(\hat{R}_0, \hat{\rho}_0) = (0.1, 0.5)$  and time horizon  $T = 100$ .

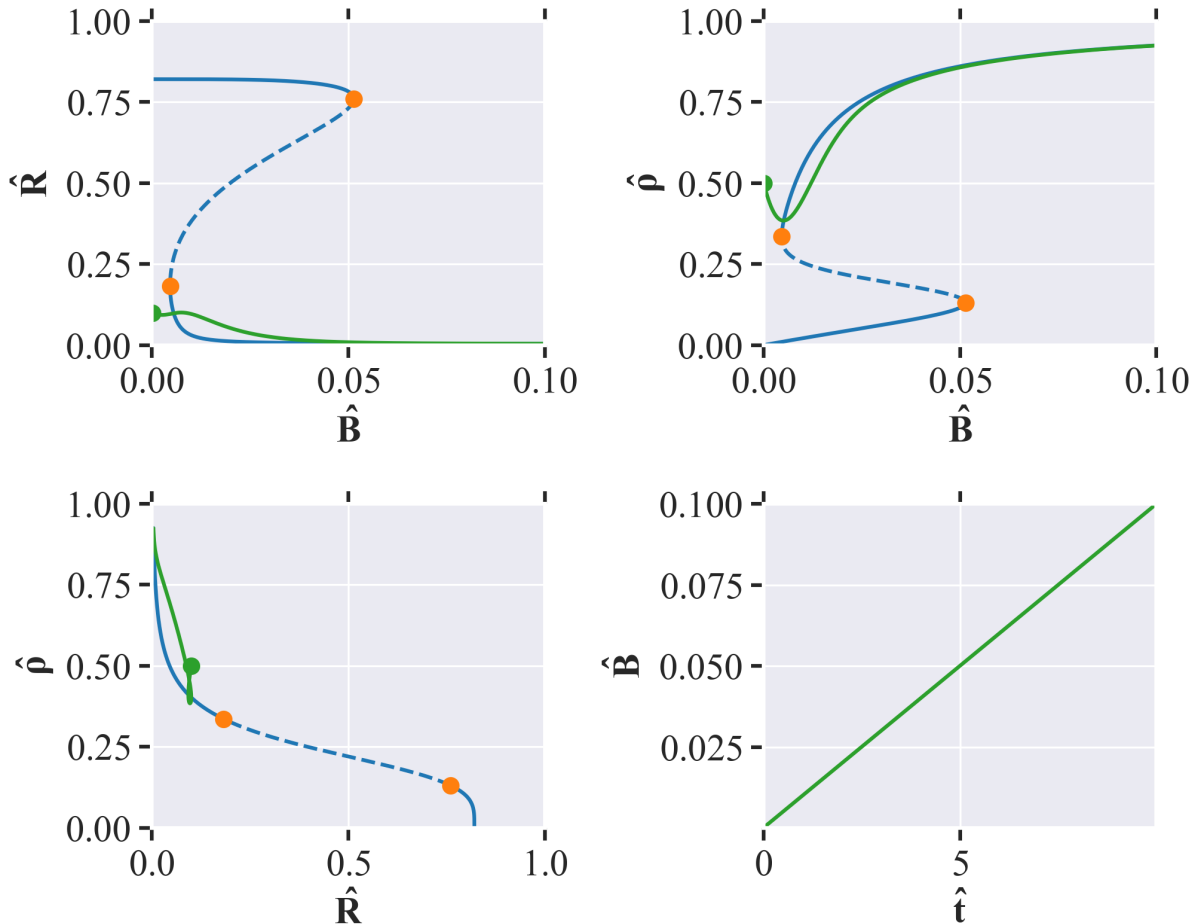


**Figure 11:** Equivalent to figure 10, but now for big  $\epsilon = 0.01$  and time horizon  $T = 10$ .

Next, we look for critical slowing down near the bifurcations of the system. The results for  $\epsilon = 0.001$  and  $\epsilon = 0.01$  are shown in figures 12 and 13 respectively.

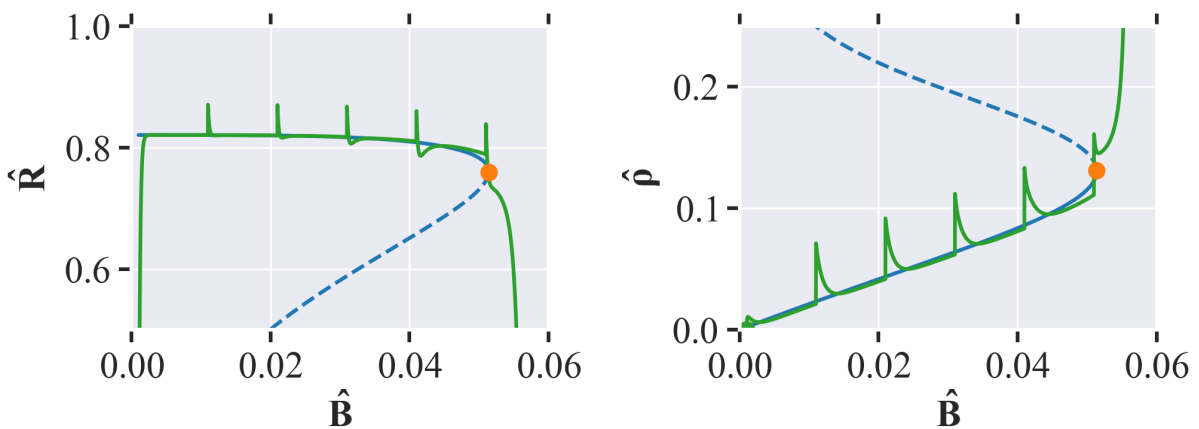


**Figure 12:** System behavior as it nears a turning point and under artificially added perturbations for  $\epsilon = 0.001$ . The perturbations are sufficiently small and sparse in time to allow the system to restore to its equilibrium.

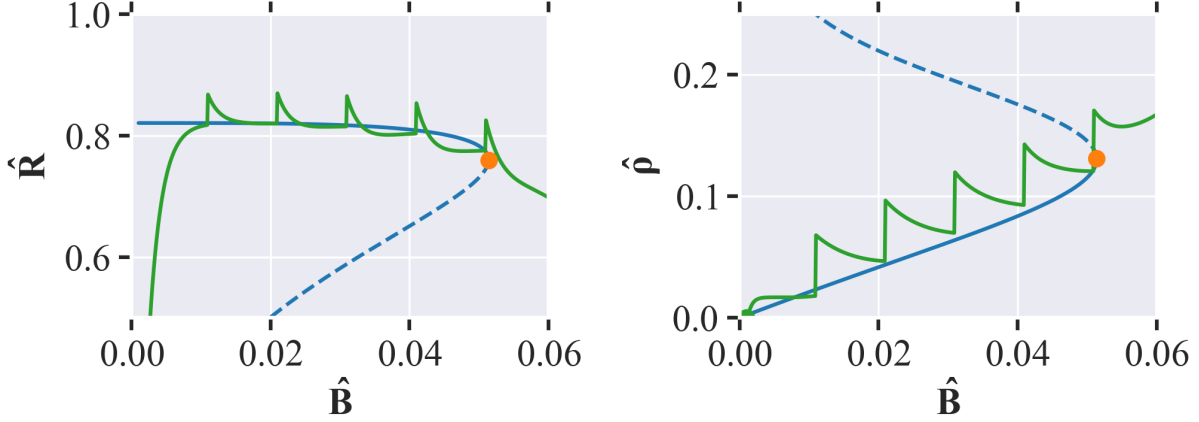


**Figure 13:** Exactly the same as figure 12, but now for  $\epsilon = 0.01$ . The perturbations are also the same, but are now too large and too frequent for the system to fully restore to its equilibrium.

In both Figures 12 and 13, we see that the system slows down in its convergence to the equilibrium near the turning point. As a consequence, the system is more sensitive to perturbations near the turning point. This is a clear example of critical slowing down. We also see that the system is more sensitive to perturbations when  $\epsilon$  is larger. This is because the system has less time to restore to its equilibrium before the next perturbation is applied. In other words, the critical slowing down is more pronounced when  $\epsilon$  is larger. Additionally, the final perturbation just before the turning point in all cases even causes the system to diverge from the equilibrium. This is because the system is already close to the turning point and the perturbation is too large to allow the system to restore to its equilibrium. Lastly,  $\hat{R}_a$  seems to be more affected by this critical slowing down than  $\hat{\rho}_a$ .

The findings in this section are in line with the theory on critical slowing down. Indeed, as a system nears a bifurcation point, the eigenvalues of the corresponding linearized system approach zero. The restoration time of the system is related to the reciprocal of these eigenvalues. As a result, the system slows down near the bifurcation point. This is exactly what we observe in the figures above.

### 3.4 R-tipping

We now introduce a super-linear time-dependent perturbation to  $\hat{B}$ . That is, the perturbed system is now given by

$$\begin{cases} \hat{R}'_a &= \frac{\hat{A}(1-\hat{R}_a)}{\hat{\rho}_a^n + \rho_0^n} - \hat{\delta}_R \hat{R}_a \\ \hat{\rho}'_a &= \frac{\hat{B}(1-\hat{\rho}_a)}{\hat{R}_a^n + \hat{R}_a^n} - \hat{\rho}_a \\ \hat{B}' &= \epsilon \frac{\hat{B}_{\max} - \hat{B}}{\hat{B}_{\max}}, \end{cases} \quad (10)$$

Figures 14 and 15 show the continuation of the unperturbed system 10, as well as a trajectory of system 10 for  $\epsilon = 0.01$  and  $\epsilon = 0.1$  respectively.

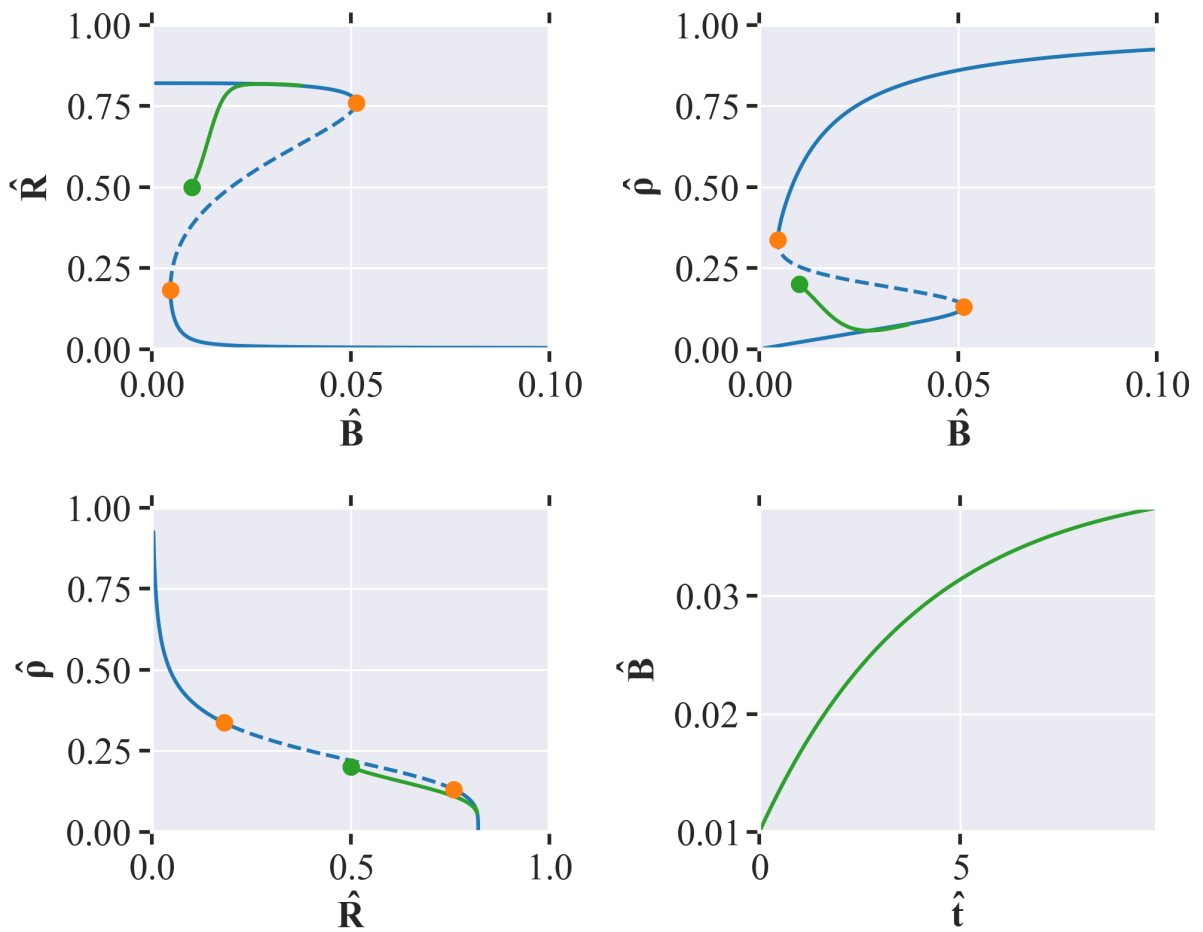


**Figure 14:** In this figure, we see the continuation of the unperturbed system 10 and a trajectory of the corresponding perturbed system for  $\epsilon = 0.01$ . The rate of the perturbation is small enough for the system to track the nearest equilibrium branch.

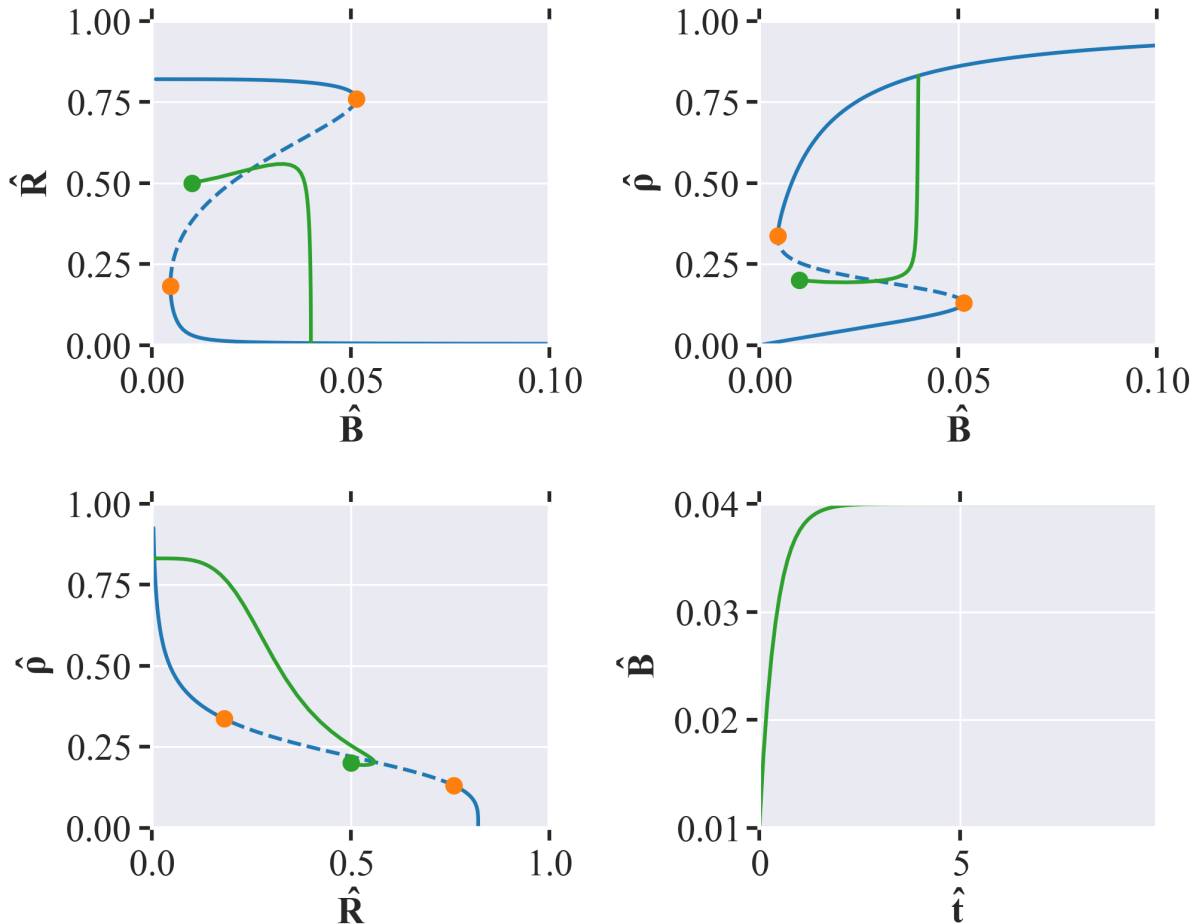


**Figure 15:** Equivalent to figure 14, but now for  $\epsilon = 0.1$ . The rate of the perturbation is now too large for the system to track the nearest equilibrium branch. Instead, the system now jumps over the unstable to the other stable equilibrium branch. This is a clear example of R-tipping.

### 3.5 Conclusion

In this assignment, we have studied the behavior of a system of ordinary differential equations that models the dynamics of a cell. We have seen that the system has two turning points, and that the system converges to one of the equilibrium points. We have also seen a case of critical slowing down. This is a situation in which the system is more sensitive to artificially added perturbations near a bifurcation point, if  $\epsilon$  (the rate of the parameter increase) is large compared to system dynamics (reciprocal of the linearized system's eigenvalues). These perturbations can cause the system to diverge from the equilibrium. Lastly, we have observed R-tipping, in which a system can jump to another equilibrium branch for  $\epsilon \approx 0.1$  and larger.